Observations of the Interaction between Cumulus Clouds and Warm Stratocumulus Clouds in the Marine Boundary Layer during ASTEX

G. M. MARTIN AND D. W. JOHNSON

U. K. Meteorological Office, Meteorological Research Flight, Farnborough, England

D. P. ROGERS

Scripps Institution of Oceanography, La Jolla, California

P. R. JONAS

Department of Atmospheric Physics, UMIST, Manchester, England

P. MINNIS

NASA/Langley Research Center, Hampton, Virginia

D. A. HEGG

Department of Atmospheric Sciences, University of Washington, Seattle, Washington

(Manuscript received 1 June 1994, in final form 20 October 1994)

ABSTRACT

Decoupling of the marine boundary layer beneath stratocumulus clouds and the formation of cumulus clouds at the top of a surface-based mixed layer (SML) have frequently been observed and modeled. When such cumulus clouds penetrate the overlying stratocumulus layer, the cloud microphysics and hence the radiative properties of the cloud are altered locally. Observations made during a series of Lagrangian experiments in the Azores as part of the Atlantic Stratocumulus Transition Experiment (ASTEX, June 1992) have been analyzed to ascertain how the properties of a stratocumulus layer with which cumulus clouds are interacting differ from those of an unaffected cloud layer. The results suggest that in regions where cumulus clouds penetrate the cloud layer, the stratocumulus is thickened as the cumuli spread out into its base. Transport of air from the SML into the cloud by convective updrafts is observed, and the increase in available moisture within the penetrating cumulus clouds results in increased liquid water content and hence changes in the droplet size spectra. The greater liquid water path results in a larger cloud optical depth, so that regions where cumulus are interacting with the stratocumulus layer can be observed in satellite measurements. Therefore, it is likely that the surface energy budget may be significantly altered by this process, and it may be necessary to parameterize these effects in large-scale numerical models.

1. Introduction

Marine stratocumulus clouds have an important influence on the global radiation budget and consequently the earth's climate. Their large horizontal extent and high albedo relative to that of the sea surface mean that it is important to understand the processes that control the radiative properties of these cloud layers. Extensive semipermanent sheets of marine stratocumulus are located off the western coasts of North and South America and the southern part of the African continent. In these regions, strong subsidence associated with the subtropical anticyclones occurs over the relatively cool ocean currents, and stratocumulus clouds form beneath the resulting temperature inversion. Although the most persistent stratocumulus sheets are found in these regions, there are several other significant areas of marine stratocumulus clouds. In the area around the United Kingdom, stratocumulus is by far the most often reported cloud type (Nicholls 1984).

Simple descriptions of marine stratocumulus clouds (e.g., Hanson 1991; Nicholls 1984; Nicholls and Leighton 1986; Rogers and Telford 1986; Nicholls 1987) show a uniformly thick cloud layer forming at the top of the marine boundary layer beneath a subsi-

Corresponding author address: Dr. G. M. Martin, Meteorological Office, Meteorological Research Flight, Building Y46, DRA Farnborough, Hampshire, GU14 6TD, England.

dence inversion. The cloud layers are opaque to infrared radiation and radiate almost as blackbodies. The resulting radiative cooling from the cloud top generates turbulent mixing that maintains the entire depth of the boundary layer in a vertically well-mixed state. Many observations of such homogeneous cloud layers have been made (Nicholls 1984; Nicholls and Leighton 1986; Slingo et al. 1982; Bower and Choularton 1992; Martin et al. 1994). However, a common observation in cloud-topped marine boundary layers is the presence of cumulus clouds forming below the stratocumulus and rising up into it (James 1959; Nicholls 1984; Paluch and Lenschow 1991; Foot 1988; Slingo et al. 1982; Nicholls et al. 1983). This situation can arise when the boundary layer becomes decoupled, such that the layer in which the stratocumulus exists (the decoupled mixed layer) is detached from the surface-based mixed layer (SML) by a stable layer, which marks the lower boundary of mixing generated by cloud-top radiative cooling (Nicholls 1984; Albrecht et al. 1985; Nicholls and Leighton 1986; Turton and Nicholls 1987; Albrecht et al. 1988; Paluch and Lenschow 1991; Hanson 1991). Decoupling can occur as a result of shortwave heating within the cloud layer (Slingo et al. 1982; Nicholls 1984; Rogers and Koračin 1992), in which case it often exhibits a marked diurnal cycle (Bougeault 1985), or from evaporation of drizzle beneath the stratocumulus cloud base (Albrecht 1989; Nicholls 1984). Both of these effects have a stabilising influence on mixing throughout the boundary layer, impeding the transfer of turbulent kinetic energy from the cloud top to the surface. It has also been suggested (Turton and Nicholls 1987) that changes in the amount of large-scale subsidence in the free troposphere may determine the boundary-layer structure. Their model predicts that if large-scale subsidence decreases, the cloud top will rise due to entrainment driven by cloud-related processes and the boundary layer may become more or less permanently decoupled as it becomes too deep to maintain a well-mixed state.

The effect of decoupling on the stratocumulus cloud is to virtually cut off the cloud layer from the moisture source of the sea surface. Entrainment of warmer dry air from above the temperature inversion into the cloud will no longer be balanced by an upward moisture flux, so the cloud layer may thin and break up. Meanwhile, the surface fluxes of heat and moisture cause the relative humidity in the SML to increase, and cumulus clouds form when the SML becomes conditionally unstable (Paluch and Lenschow 1991; Nicholls 1984). They rise up into the stratocumulus layer above, and it has been suggested (Nicholls 1984) that such clouds could act to link the cloud layer and SML. The local enhancement of the moisture flux could counteract the thinning of the stratocumulus layer, as shown by Bougeault (1985), resulting in higher liquid water contents (Nicholls 1984). Rogers et al. (1994b) suggest that cumulus clouds could help to enhance stratocumulus cloud formation in the nighttime radiatively cooled boundary layer.

If cumulus clouds do form in a decoupled boundary layer beneath a stratocumulus deck, they may significantly affect both the structure of the boundary layer by latent heat release and, if they penetrate the overlying cloud layer, the microphysics of the stratocumulus, due to their substantially different dynamics (Nicholls 1984). The vertical motions associated with stratocumulus clouds are typically less than 1 $m\ s^{-1}$ (Rogers and Yau 1989), thus limiting the supersaturation to about 0.3% (Martin et al. 1994). Although stratocumulus clouds are turbulent, the vertical velocities associated with cumulus clouds are generally higher than in stratocumulus clouds, so that significant entrainment and mixing with the surrounding unsaturated air occurs during their growth. The effects of the mixing of cloudy air with drier environmental air on the cloud microphysics are still a matter for debate, and much observational and modeling work has been devoted to this problem (Blyth 1993). However, it is likely that the intrusion of cumulus clouds into a stratocumulus layer will have a marked effect on the microphysics of the stratocumulus. The introduction of a different droplet size distribution, which includes large drops, could initiate or enhance coalescence in the cloud layer. Entrainment of free tropospheric air into the stratocumulus may be enhanced, especially if the cumulus clouds protrude above the stratocumulus and locally distort the inversion, and this may further alter the stratocumulus microphysics.

Nicholls (1984) suggested that although the cumulus clouds may provide a link between the moisture source in the surface-based mixed layer and the decoupled cloud layer, and so help to maintain the stratocumulus, increased entrainment of dry free tropospheric air into the stratocumulus due to penetration of vigorous cumulus clouds could result in rapid break up of the cloud layer. It has been suggested (Bretherton 1992) that the observed transition from stratocumulus to trade wind cumulus in the subtropics may be a result of the latter process. The subtropical marine boundary layer will experience decreasing large-scale subsidence as the air moves southward, and the increase in sea surface temperature relative to the temperature just above the inversion will cause the cloud top to rise, resulting in permanent decoupling. The resulting drying of the cloud layer by continued entrainment, enhanced by the penetration of relatively vigorous cumulus clouds, may lead to dissipation of the stratocumulus, exposing the underlying cumulus clouds. Johnson et al. (1994) suggest that when the cumulus clouds are less vigorous they may actually maintain the stratocumulus, so that in the subtropics it will persist for longer than it would if there were no cumulus clouds present.

It is apparent from the preceding discussion that the interaction between cumulus and stratocumulus clouds in a decoupled boundary layer may be of considerable

importance, not only in altering the microphysics and hence the radiative properties of the cloud layer, but also in either maintaining the layer throughout the diurnal cycle or causing it to dissipate by enhancing cloud-top entrainment. If this interaction is inherent in the transition of stratocumulus to trade wind cumulus, then it may also have implications for the global climate. The aims of the Atlantic Stratocumulus Transition Experiment (ASTEX), which took place in the Azores in June 1992 (Albrecht et al. 1994), were to ascertain the physical processes responsible for the transition from stratocumulus clouds to shallow trade wind cumulus clouds and the consequence of this transition for the atmosphere and the ocean. During ASTEX, the cloud type most frequently observed was that of cumulus rising into stratocumulus. Extensive, homogeneous cloud sheets were not observed, and the cloud layers varied in thickness and extent. Often, the thickest cloud appeared to be associated with the presence of penetrating cumulus clouds.

One of the major objectives of ASTEX (in collaboration with the Marine Aerosol and Gas Exchange experiment) was to study the evolution of the boundary layer and to observe changes in the cloud characteristics associated with it using a series of Lagrangian experiments. Constant level balloons carrying Global Positioning System locators were launched from a ship into the boundary layer in the north of the ASTEX triangle (see Albrecht et al. 1994), and aircraft were sent out sequentially from Santa Maria, in the Azores (at the northern vertex of the triangle), to make measurements in the same air mass as the balloons. An attempt was made in each experiment to have at least one aircraft in the same air mass almost continuously for a full 48-h period. Two such series of experiments were performed, and although many of the balloons were lost in the sea it was found possible to remain in approximately the same air mass for the full period in both cases, by tracking the remaining balloons, using model trajectories as guidance, and allowing the aircraft flight tracks to drift with the wind in the boundary layer. This paper summarizes observations of the cumulus–stratocumulus interaction made over a 34-h period during the second series of Lagrangian experiments, from 0500 UTC 19 June 1992 to 1500 UTC 20 June 1992. Results from three aircraft and satellite measurements are used in this study.

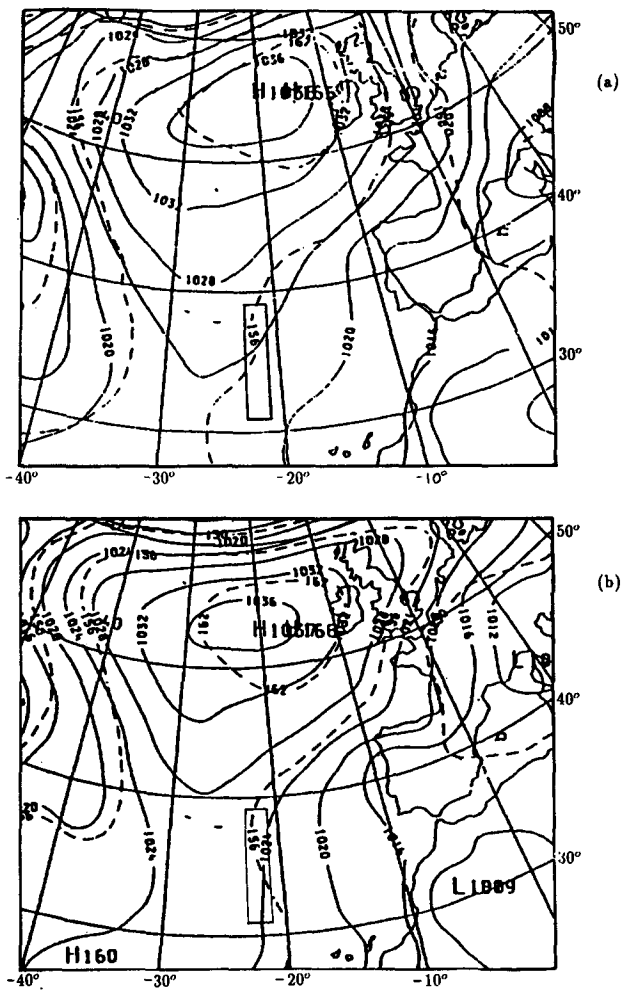

FIG. 1. Synoptic situation on (a) 19 June 1992 and (b) 20 June 1992 at 0000 UTC. Mean sea level pressure (solid) and 850-mb heights (dashed). Box indicates operating area.

2. The Lagrangian experiment 19–20 June 1992

a. Synoptic situation

The synoptic situation is shown in Fig. 1a,b. A surface high pressure region was centered over the Atlantic, just west of Ireland, so that the flow through the operating area (indicated by the box) was northeasterly. An upper-level trough was present to the east of Santa Maria (37.0°N, 25.2°W), bringing cirrus and altocumulus to the region. This can be seen from the Meteosat infrared images from 0030 UTC on 19 and 20 June in Fig. 2. The upper-level disturbance moved northward during the day, but the low-level clouds moved southwestward. Observations made during the previous four days had shown the presence of a large plume of highly polluted continental air, which appeared to have originated over northwest Europe, moving southwestward through the region (Johnson et al. 1993). A relatively sharp transition existed between this continental air mass and the maritime air mass that had originated over the center of the Atlantic Ocean. Figures 3a,b, which show 1000- and 700-mb isentropic back trajectories for the 72-h leading up to the start of the experiment [calculated using European Centre for Medium-Range Weather Forecasts (ECMWF) analyses], confirm that this experiment took place almost entirely in the continental air mass. The free tropospheric air has been affected by circulations around the

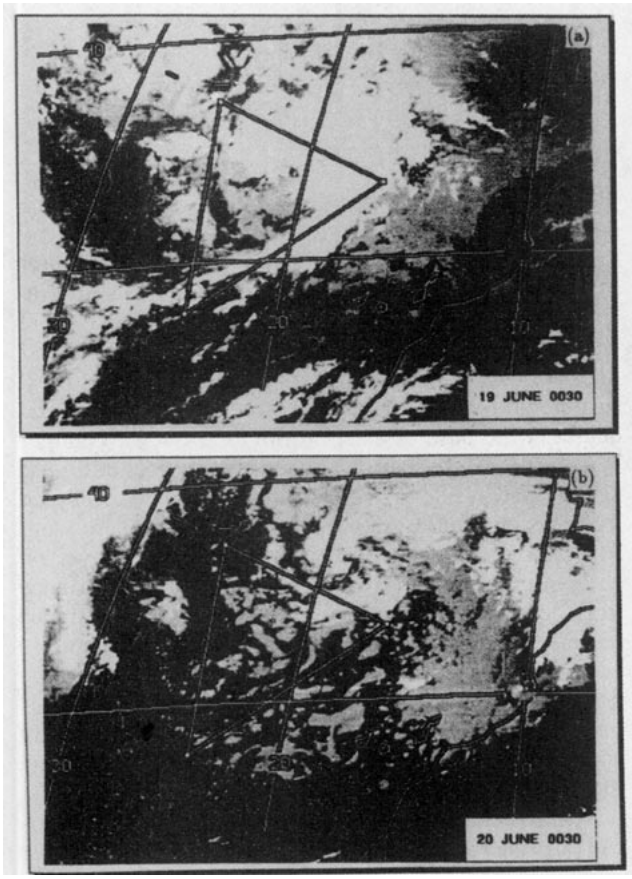

FIG. 2. Meteosat infrared satellite images for (a) 19 June 1992 and (b) 20 June 1992, at 0030 UTC. The ASTEX triangle is shown (from Bluth and Albrecht 1993).

upper low, but the boundary-layer air has clearly come from northern Europe and is therefore likely to show significant continental characteristics.

b. *Platforms*

The details of this experiment are summarized by Albrecht et al. (1994). Three aircraft—the National Center for Atmospheric Research (NCAR) Electra, the Meteorological Research Flight (MRF) C-130, and the University of Washington (UW) C-131—were used to track the movement of a centroid of three constant level balloons, which had been released into the boundary layer from the National Oceanic and Atmospheric Administration's *Oceanus* research ship at 38.2°N, 21.5°W at 2200 UTC on 18 June. Each aircraft measured

(a) standard meteorological parameters (e.g., temperature, dew point, wind speed and direction, and humidity);

(b) cloud physics and aerosol parameters—droplet and particle concentrations and sizes; and

(c) radiation parameters—broadband and narrowband radiances and cloud-top and sea surface temperatures.

Details of the instrumentation on each of the three aircraft are given in Miller and Friesen (1989) for the NCAR Electra, Rogers et al. (1995a) for the MRF C-130, and Hobbs et al. (1991) for the UW C-131. A number of side-by-side intercomparisons were made between the Electra and the C-130 during ASTEX, and these revealed small discrepancies between the measurements made by the two aircraft. No side-by-side intercomparisons were made with the C-131. However, the data from all three aircraft are used in this study to illustrate the overall changes in the boundary-layer structure and the cloud microphysics, and we assume that any small discrepancies between the measurements made by the different aircraft will not affect the conclusions drawn in this paper.

c. *Aircraft flight patterns*

The flight patterns made by each of the aircraft consisted of

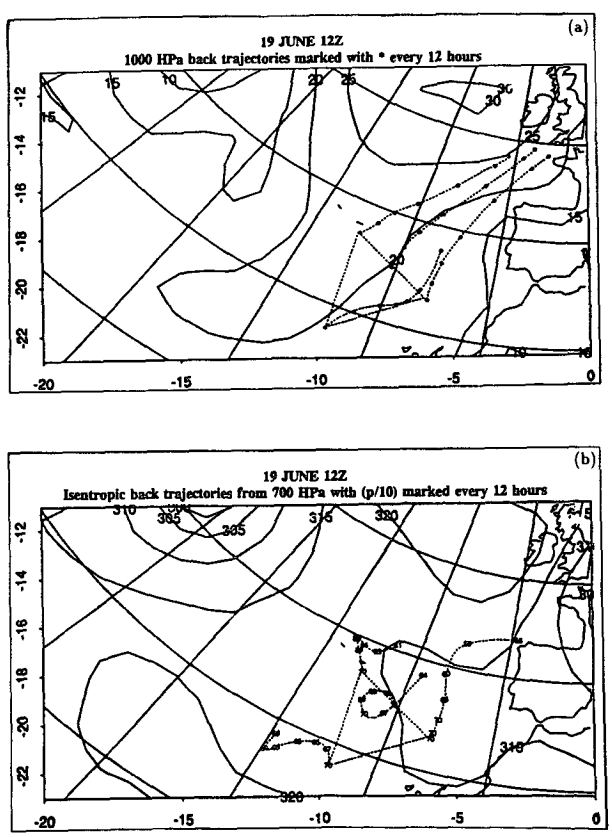

FIG. 3. (a) Isobaric back trajectories, calculated using ECMWF analyses at 1000 mb, and (b) isentropic back trajectories from the 700-mb surface for the 72 h before 1200 UTC on 19 June 1992. The contours in (a) are the surface pressure and those in (b) are potential temperature (from Bluth and Albrecht 1993).

(a) slow ascents or descents (2.5 m s^{-1} in the boundary layer, 5 m s^{-1} in the free troposphere), between several hundred meters above the temperature inversion and 15 m above the sea surface, to provide profiles of the boundary layer and

(b) a number of vertical stacks, with each made up of several 10- or 20-min straight and level runs, between 80 and 100 m s^{-1}, at different altitudes. The run heights were chosen so that each of the layers within the boundary layer was sampled, and there was usually one run above cloud in the free troposphere. Often, a run "porpoising" up and down from approximately 100 m above cloud top to 100 m below cloud top was made, at a descent/ascent rate of 1 m s^{-1}, to try to determine the entrainment rate at the top of the boundary layer.

This allowed both the vertical structure and the horizontal variability in the boundary layer to be determined. The horizontal runs were either made perpendicular to and drifting with the wind or in "L" patterns with crosswind and downwind legs also drifting with the wind. The flight tracks of the three aircraft, together with the trajectory followed by the balloons, are shown in Fig. 4.

3. Aircraft measurements

The characteristics of the stratocumulus clouds were observed to change considerably over the 34-h period. The next sections give a detailed description of the boundary-layer structure and the stratocumulus microphysics as observed by the aircraft.

a. Boundary-layer structure

Figures 5 and 6 show series of profiles of equivalent potential temperature (θ_e) and total water content (q_T) measured during the Lagrangian experiment. (Figures 5f and 6f are made up of four horizontal runs and include the interim ascents to each level because there was no profile in the operating area during the C-131 flight.) Each of the parameters is plotted against pressure height, which has been corrected using the radar height at the base of each profile to allow for changes in the surface pressure. The droplet concentration is also plotted in Fig. 5, to show where cloud was sampled during each profile. An attempt has been made to identify the different layers within the boundary layer on each of these profiles, based on the relative invariance of θ_e and q_T within each layer. The horizontal distance traveled during a profile (several tens of kilometers) and the considerable lateral variability within the boundary layer mean that the heights of the boundaries between each of the layers at a particular time are only approximate. However, they are used here to illustrate the vertical structure of the boundary layer.

The boundary layer is clearly not well mixed vertically. Higher values of θ_e are seen in the lowest layer

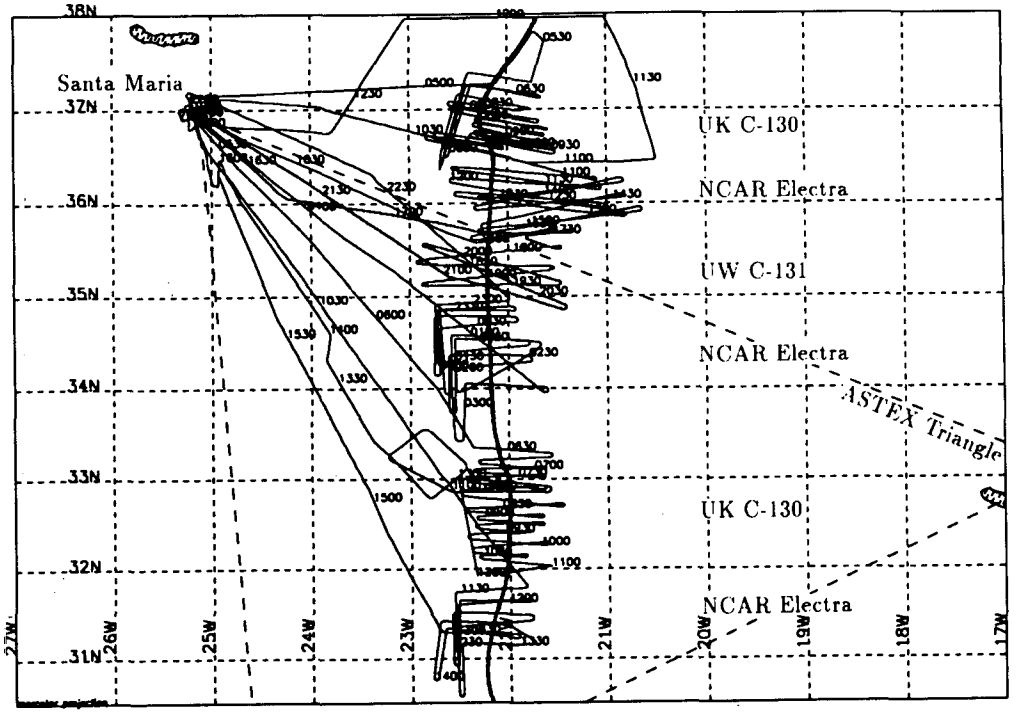

FIG. 4. Flight tracks of the MRF C-130, NCAR *Electra*, and UW C-131 during 19–20 June 1992. The thick line indicates the balloon trajectory.

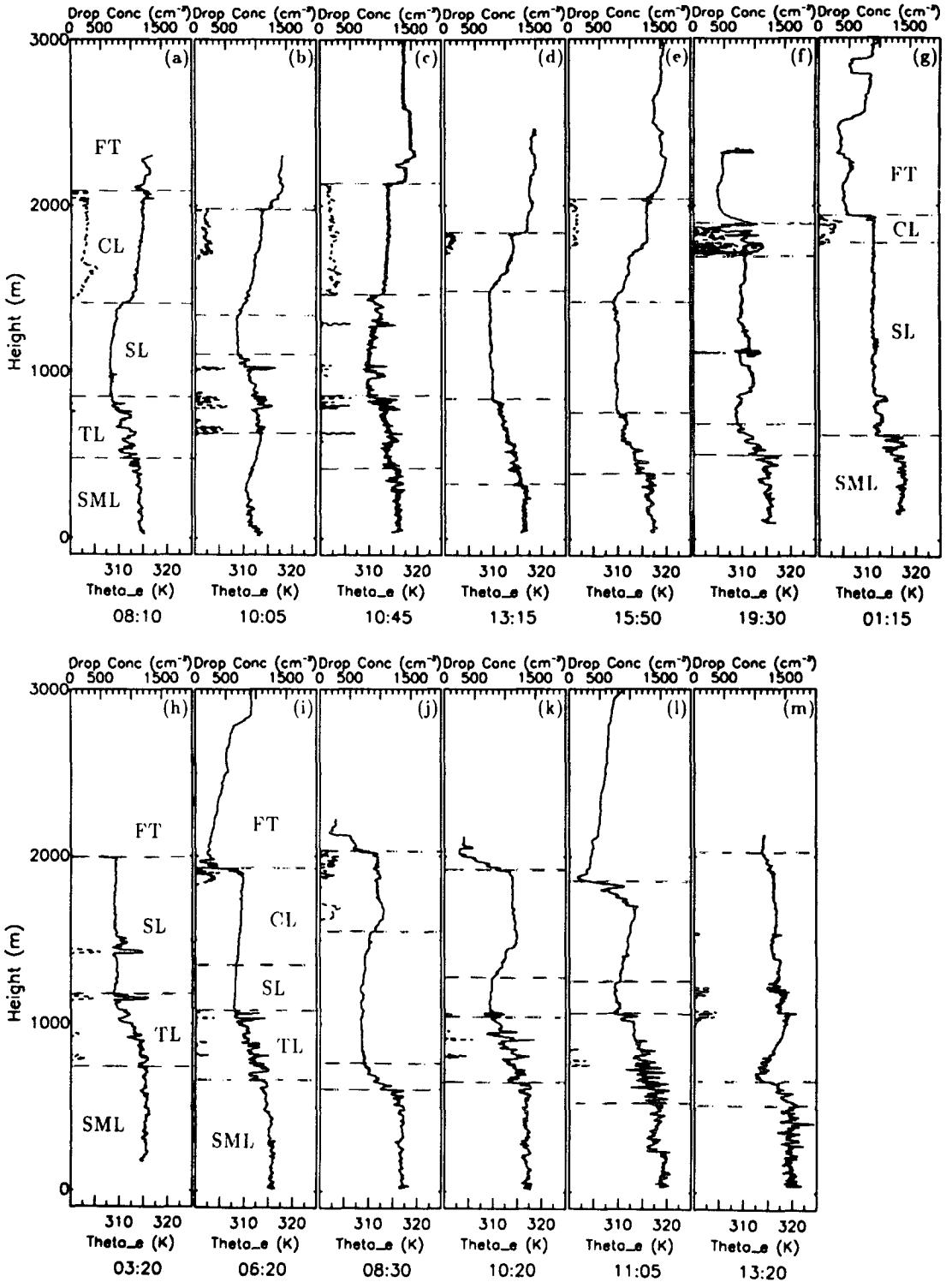

FIG. 5. Profiles of equivalent potential temperature [θ_e (K), solid line] measured by the aircraft during the Lagrangian experiment. The approximate time of the profile is given at the base of each graph. Also shown is the droplet concentration (dotted line) to indicate where cloud was sampled. The limits of the different layers within the boundary layer are indicated by the horizontal dashed lines: SML—surface mixed layer; TL—transition layer; SL—subcloud layer; CL—cloud layer; and FT—free troposphere.

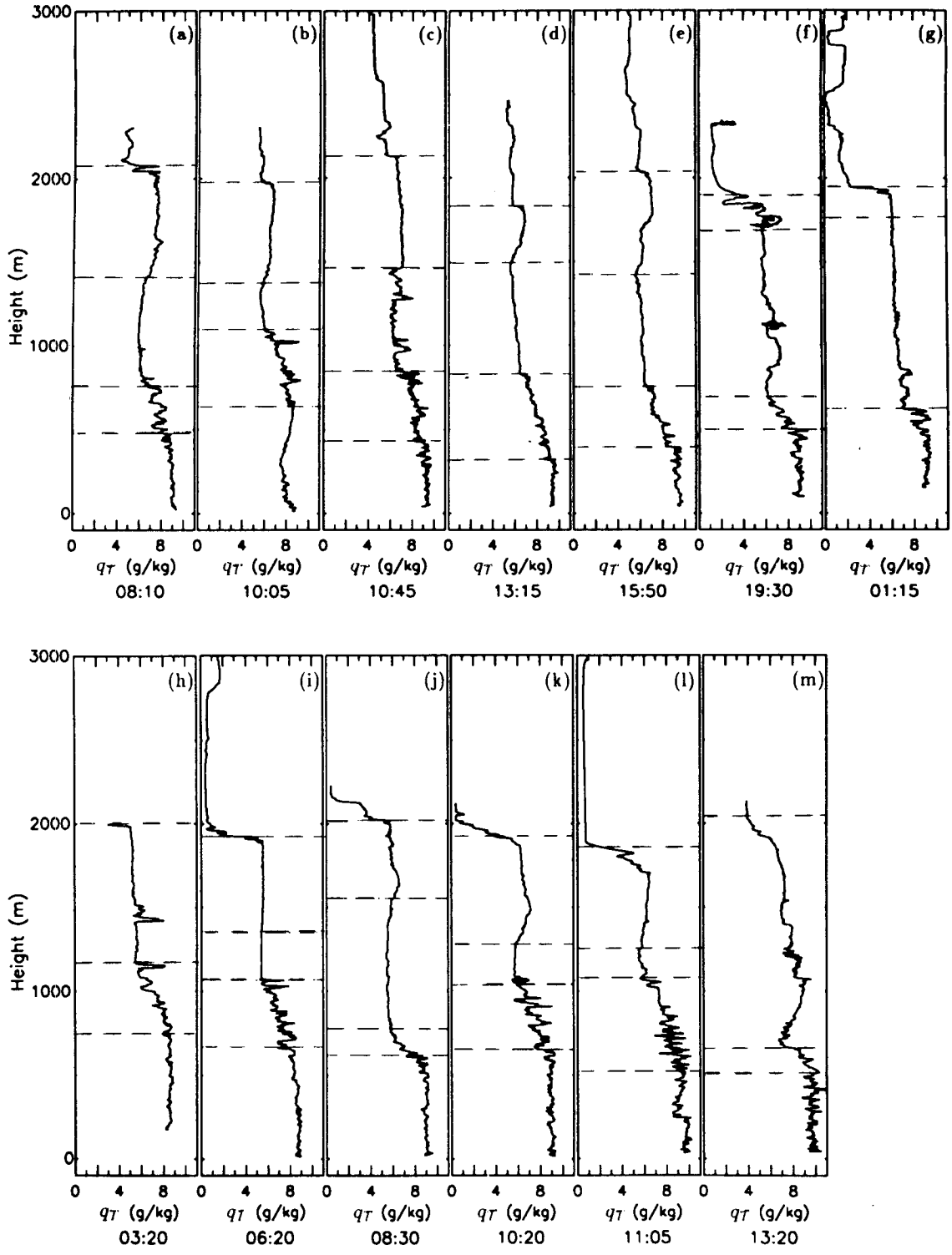

FIG. 6. Profiles of total water content (q_T, g kg^{-1}) measured by the aircraft during the Lagrangian experiment. The different layers within the boundary layer are indicated as in Fig. 5.

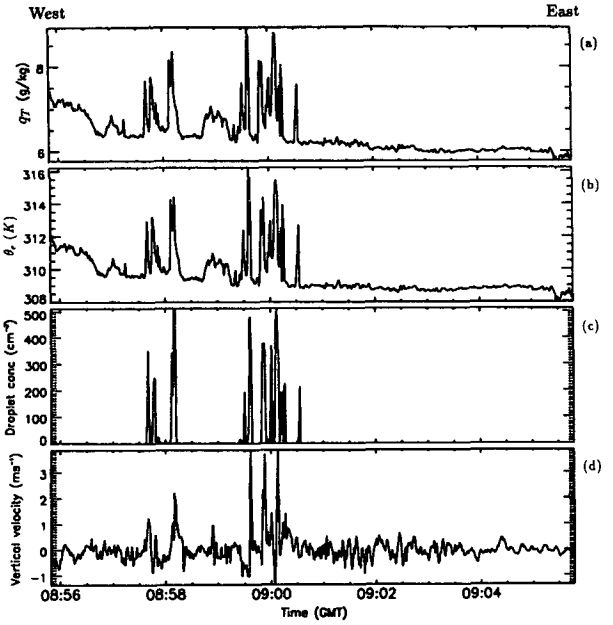

FIG. 7. Measurements made during a straight and level run below the stratocumulus at 0900 UTC on 19 June 1992 at a height of 1065 m: (a) q_T (g kg^{-1}), (b) θ_e (K), (c) droplet concentration (cm^{-3}), and (d) vertical velocity (m s^{-1}).

(the SML) than in the layers above. There is often a transition layer of varying thickness between the SML and a drier lower θ_e layer below the stratocumulus, termed the subcloud layer. The profiles of droplet concentration show where cumulus clouds below the stratocumulus were penetrated in these layers during the profiles. The stratocumulus itself varies in thickness, and several profiles do not pass through the cloud layer, indicating that its horizontal extent also varies. Where there is stratocumulus, the values of θ_e and q_T within the cloud layer are often higher than in the subcloud layer, so that mixing between these two layers will be inhibited.

One of the most noticeable changes that occurred during this Lagrangian experiment was in the maximum depth of cumulus clouds forming at the top of the SML and rising up into the cloud layer. Visual observations indicated that the number of cumulus clouds large enough to penetrate the stratocumulus layer decreased substantially through the afternoon of 19 June, reaching a minimum in the early morning of 20 June so that by 0600 UTC none of the cumulus cloud tops were reaching the stratocumulus base, and then increasing again through the day. It is therefore possible to study the differences in the boundary-layer structure and the stratocumulus microphysics in the two regimes.

Although the inherently turbulent nature of cumulus clouds means that substantial mixing occurs between these clouds and the environment, it is likely that the air carried with a cumulus cloud that penetrates a stratocumulus cloud layer will be strongly influenced by the characteristics of the SML. Figure 7 shows measurements of q_T, θ_e, droplet concentration, and vertical velocity made during a straight and level run below the stratocumulus on 19 June at 0900 UTC. The graphs of droplet concentration and vertical velocity show the presence of active cumulus clouds, which were observed to be penetrating the overlying stratocumulus layer. Corresponding spikes are seen in q_T and θ_e and comparison with Figs. 5a and 6a reveals that these high values are characteristic of the SML air, while the lower background values are similar to those in the subcloud layer. Similar observations were made in other runs through cumulus clouds during this experiment, and this evidence suggests that the cumuli were distinct from the stratocumulus and that where the cumulus clouds were penetrating the stratocumulus they were transporting SML air into the upper cloud layer. Figure 8 shows measurements of q_T, θ_e, droplet concentration, and vertical velocity during a horizontal run through stratocumulus at 0730 UTC on 19 June. The arrows on Fig. 8d highlight where spikes in the vertical velocity indicate that cumulus clouds are penetrating the stratocumulus, and corresponding increases in θ_e and q_T are seen. Comparison with Figs. 5a and 6a shows that the maxima are once again characteristic of the SML air. However, these increases do not appear as sharp as those seen in Fig. 8, because the background values in the stratocumulus are far higher than those in the subcloud layer.

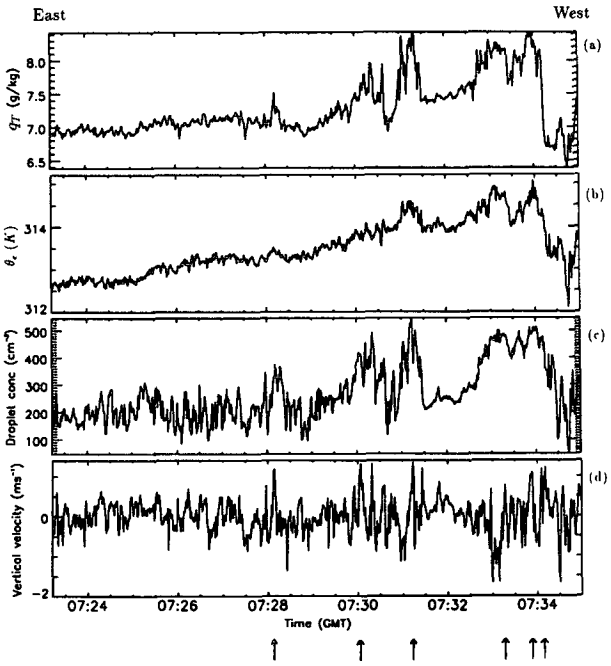

FIG. 8. As in Fig. 7 but for a run in the stratocumulus at 0730 UTC on 19 June at a height of 1700 m. Arrows indicate active updrafts associated with cumulus cloud penetration.

Further insight into possible processes occurring in this boundary layer can be gained using the mixing diagram (Paluch 1979) in Fig. 9a. This is a composite of 1-s values from a vertical stack of horizontal runs on 19 June between 0820 and 0954 UTC. The lowest run was through the SML, and the next was through the transition region. Several of the runs in the subcloud layer penetrated cumulus clouds. One run was through the main cloud layer, another in the free tropospheric air, and one run porpoised through the cloud top, sampling both cloudy air and free tropospheric air. Where cloud has been sampled, the 1-s values of θ_e and q_T are overplotted with a symbol, the symbols being different for each of the runs at different heights. The regions on the diagram corresponding to each of the layers described above have been identified by comparing the horizontal runs with the profiles in Figs. 5 and 6, and are labeled on the diagram. Region A represents the SML air, with high values of θ_e and q_T. Region C denotes the sub-cloud-layer air, where the values of θ_e and q_T are significantly lower, and region B indicates the transition region between the SML and the subcloud layer. Region E represents the stratocumulus cloud layer, and region H is the free tropospheric air. The points in region G denote air sampled just at the cloud top during the porpoise run and indicate that mixing between the boundary-layer air and the free tropospheric air has occurred. The air associated with the stratocumulus cloud (E) appears to be a mixture of air from the SML, the subcloud layer, and the free troposphere. The cloudy points in Region F are from active cumulus clouds penetrating the stratocumulus. The position of these points suggests that this air has recently come from the SML, but some mixing between the cumulus and stratocumulus has occurred. Similarly, the cloudy points between A and B (regions labeled D) are from cumulus clouds at various stages of development, sampled at different heights in the subcloud layer. The positions of these points on the diagram imply that different amounts of mixing have taken place between the SML and sub-cloud-layer air.

Regions A–H have also been identified on the mixing diagrams in Figs. 9b–e. During the period between midday and sunset on 19 June, cumulus clouds were observed to spread out below the base of the stratocumulus, forming a patchy lower cloud layer. This lower layer began to dissipate toward evening, as the maximum depth of the cumulus clouds decreased. Overnight, the stratocumulus layer thickened as the longwave cooling at the cloud top was no longer offset by shortwave heating, but the cumulus clouds began to spread out again at the lower level the next morning as their maximum depths increased. Cloudy points from the patches of cloud formed by spreading out of the cumulus clouds below the stratocumulus base are denoted in Figs. 9b, 9c, and 9e by region I. These cloud patches show a greater influence of the SML than the main stratocumulus cloud layer. This is particularly well marked in Fig. 9e at 1120–1309 UTC on 20 June.

The mixing diagrams in Figs. 9a–e show a significant change in the characteristics of the free-tropospheric air (region H) over the period. On the 19 June, the values of q_T and θ_e in this air seem more characteristic of boundary-layer air than subsiding free-tropospheric air, and it is thought that this air was associated with the continental plume described in Section 2a. Trajectory analysis carried out for the previous few days showed that this air probably originated over North Africa, being carried up into the free troposphere within a low pressure system. Observations made between 1600–0400 UTC on 19/20 June revealed considerable lateral variability in the character of this air, suggesting that there was an upper-air katafront above the boundary layer. In most of the observations after 2030 UTC on 19 June, the air immediately above the inversion was significantly drier and more characteristic of subsiding free tropospheric air. The effect on the stratocumulus of slow entrainment of this increasingly dry air is to decrease the q_T and θ_e at the top of the main cloud layer (as seen as a movement of the points in region G toward region H). The stratocumulus layer observed on the morning of 20 June was considerably thinner than that observed the day before. It is possible that entrainment of the increasingly dry air from the free troposphere into the cloud has assisted in the dissipation of the cloud.

b. Cloud structure and microphysics

Figure 10 shows contoured cloud droplet spectra over the size range 3.2–48.7-μm diameter from two

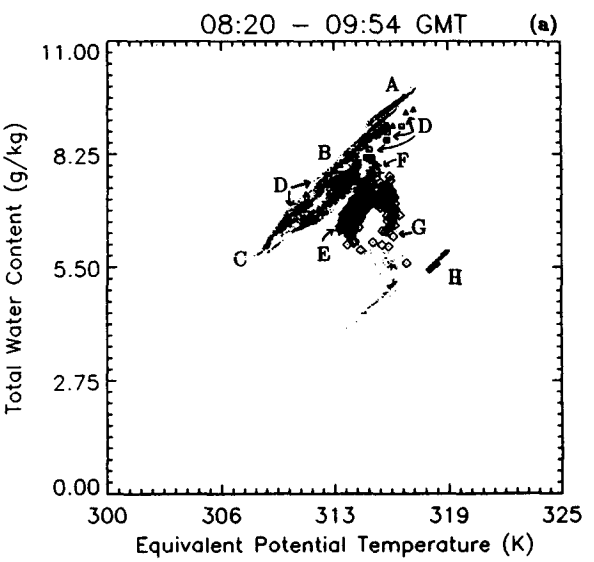

FIG. 9. Mixing diagrams of θ_e and q_T made up of vertically stacked straight and level runs in the boundary layer and just above the inversion: (a) 0820–0954 UTC 19 June 1992; (b) 1055–1304 UTC19 June 1992; (c) 2255–0122 UTC 19–20 June 1992; (d) 0626–0819 UTC 20 June 1992; and (e) 1120–1309 UTC 20 June 1992. See text for full description.

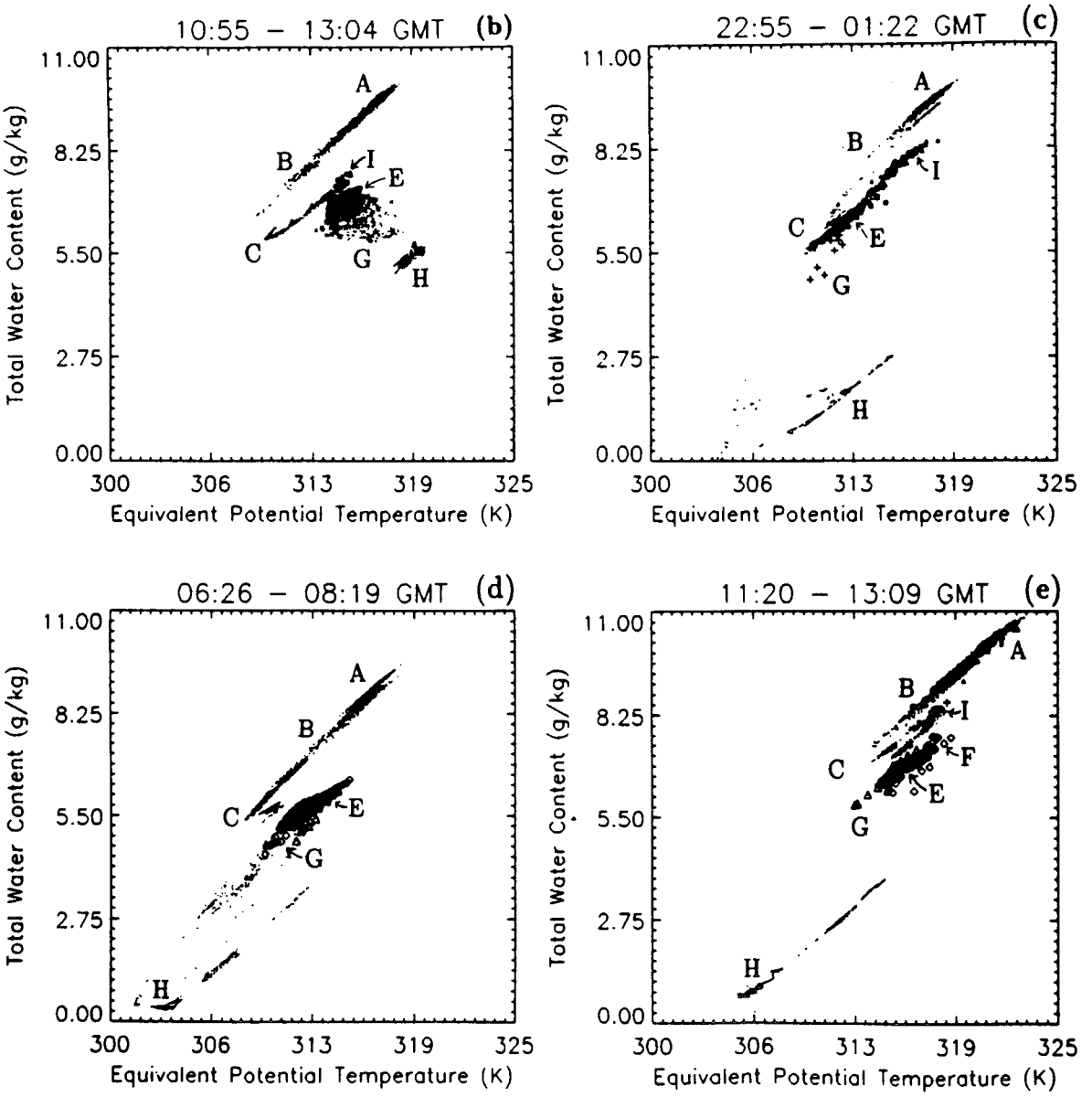

FIG. 9. (*Continued*)

horizontal runs in the stratocumulus layer: the first at 0730 UTC on 19 June, when many active cumulus clouds were penetrating the stratocumulus at the western end of the run (see Figs. 7 and 8), and the second at 0745 UTC on 20 June, when the cumulus clouds were small and did not penetrate the cloud base. The most striking difference between the two diagrams is in the range of droplet spectral shapes observed. In Fig. 10a, the mode diameter varies between 6- and 15-μm, and many of the spectra, although unimodal, have a broad, almost flattened, peak. This contour diagram corresponds to the runs shown in Fig. 8, and it can be seen that many of the broadest spectral peaks coincide with the presence of active cumulus clouds penetrating the cloud layer. In Fig. 10b, however, the spectral shape is much more uniform along the run, only changing significantly where there are holes in the cloud. These observations show that the intrusion of active cumulus clouds into the stratocumulus layer is associated with significant variations in the droplet spectral shape within the stratocumulus.

Cumulus and stratocumulus clouds are known to experience different mixing processes due to their different dynamics. Cumulus clouds generally experience considerable entrainment of the surrounding dry environmental air during their growth, due to their inher-

ently turbulent nature (Rogers and Yau 1989). The effects of mixing of cloudy air with drier environmental air on cumulus cloud microphysics are still uncertain (Blyth 1993). Generally it is agreed that entrainment is the main process by which the liquid water content in cumulus clouds becomes subadiabatic. However, much debate has been centered on the entrainment process itself and the consequence of this on the cloud droplet size distribution. Although entrainment of dry air into stratocumulus clouds does occur, observations indicate that it is mainly confined to cloud top and that much of the cloud liquid water content profile is close to adiabatic (Albrecht et al. 1985; Nicholls and Leighton 1986; Slingo et al. 1982; Noonkester 1984; Bower and Choularton 1992; Martin et al. 1994). The size distributions of droplets within each of the cloud types are therefore not expected to be the same.

In the regions where stratocumulus and cumulus clouds interact, the resultant droplet size spectrum should be a combination of that in each of the two cloud types. Thus, spectral averages such as mean droplet size may be increased or decreased locally in these regions. Figures 11a–d show the cloud droplet concentration, effective radius, liquid water content, and vertical velocity measured during the horizontal run shown in Fig. 10a. The microphysical parameters have been calculated over the same droplet size range as covered by the contour plot in Fig. 10a. The droplet effective radius is calculated from the droplet size spectrum using the following equation:

$$r_e = \frac{\int_0^\infty n(r) r^3 dr}{\int_0^\infty n(r) r^2 dr} \qquad (1)$$

(where r is the droplet radius and $n(r)dr$ is the number of droplets in the size range $r \rightarrow r + dr$ in the spectrum) and is the measure of average droplet size that characterizes the cloud optical properties (see section 4). It can be seen that where the spikes in vertical velocity indicate that cumulus clouds are penetrating the stratocumulus, the cloud droplet concentration and liquid water content are increased, but the droplet effective radius is lower. Since the effective radius calculated from a droplet size distribution is dominated by the larger droplets (because of the r^3 term), a decrease in effective radius within the penetrating cumulus clouds can be brought about by a decrease in the proportion of larger cloud droplets. Figure 10a indicates that although the spectral peak occurs at a larger diameter within the regions of active cumulus cloud penetration, the number of cloud droplets between about 28- and 48-μm diameter is actually smaller in these regions.

Figure 12 shows cloud condensation nuclei (CCN) activity spectra measured in the SML and in the subcloud layer on the morning of 19 June. It can be seen that more CCN are activated at any supersaturation in the SML than in the subcloud layer. Although cumulus clouds generally experience more entrainment than stratocumulus, which could reduce the droplet concentration by evaporation and dilution as seen in isolated cumulus clouds, the air entrained by the cumulus clouds below the stratocumulus may not be sufficiently dry to result in a significant reduction of the droplet concentration, and any such changes may only occur at the cloud top and edges, with little effect on the cloud as a whole. Thus, the droplet concentrations in these cumulus clouds may be expected to be higher than those in the stratocumulus clouds. If there are considerably more droplets competing for the available water vapor content, the maximum size to which the droplets can grow by condensation will be limited. The increased droplet concentrations in the cumulus clouds could also be a result of the higher vertical velocities typically associated with cumulus clouds compared with those of stratocumulus clouds, which could increase the maximum supersaturation and hence the number of CCN activated at the cumulus cloud base.

It is clear that the intrusion of cumulus clouds into a stratocumulus layer is associated with significant variations in the cloud microphysics. However, the size to which the droplets can grow in both the cumulus and the stratocumulus clouds will depend not only on the droplet concentration and available water vapor content but also on the cloud thickness (since droplets will have more time to grow by condensation during their passage through a thicker cloud). Therefore, the effect of an intruding cumulus cloud on the microphysics of a stratocumulus layer, as observed at a particular level above the stratocumulus base, will depend on the difference in cloud-base height between the two clouds. Observations made during a stack of horizontal runs showed that the cloud layer sampled in Fig. 10a varied in thickness laterally from about 460 m thick at the eastern end of the run to greater than 700 m thick in the region of cumulus cloud penetration at the western end of the run. Thus, the run height varied between about 150 m above the stratocumulus base at the eastern end to more than 390 m above the stratocumulus base in the region of cumulus penetration at the western end. The cumulus clouds at the western end of the run had base heights up to 650 m below the stratocumulus base, that is, up to 1040 m below the run level. The contoured droplet spectra in Fig. 10a can be contrasted with those in Fig. 13a, which are from a run at about 65 m above cloud base in a thin (less than 120 m) layer of stratocumulus between 1226 and 1236 UTC on 20 June. In much of the run, the spectra are relatively narrow, with a peak at about 4-μm diameter. However, the run passed through an active cumulus cloud at 1230 UTC, and a second peak appears in the spectrum at 15 μm. The base of the cumulus cloud in Fig. 13a was about 1000 m below the stratocumulus and therefore 1065 m below the run level, so the cumulus clouds

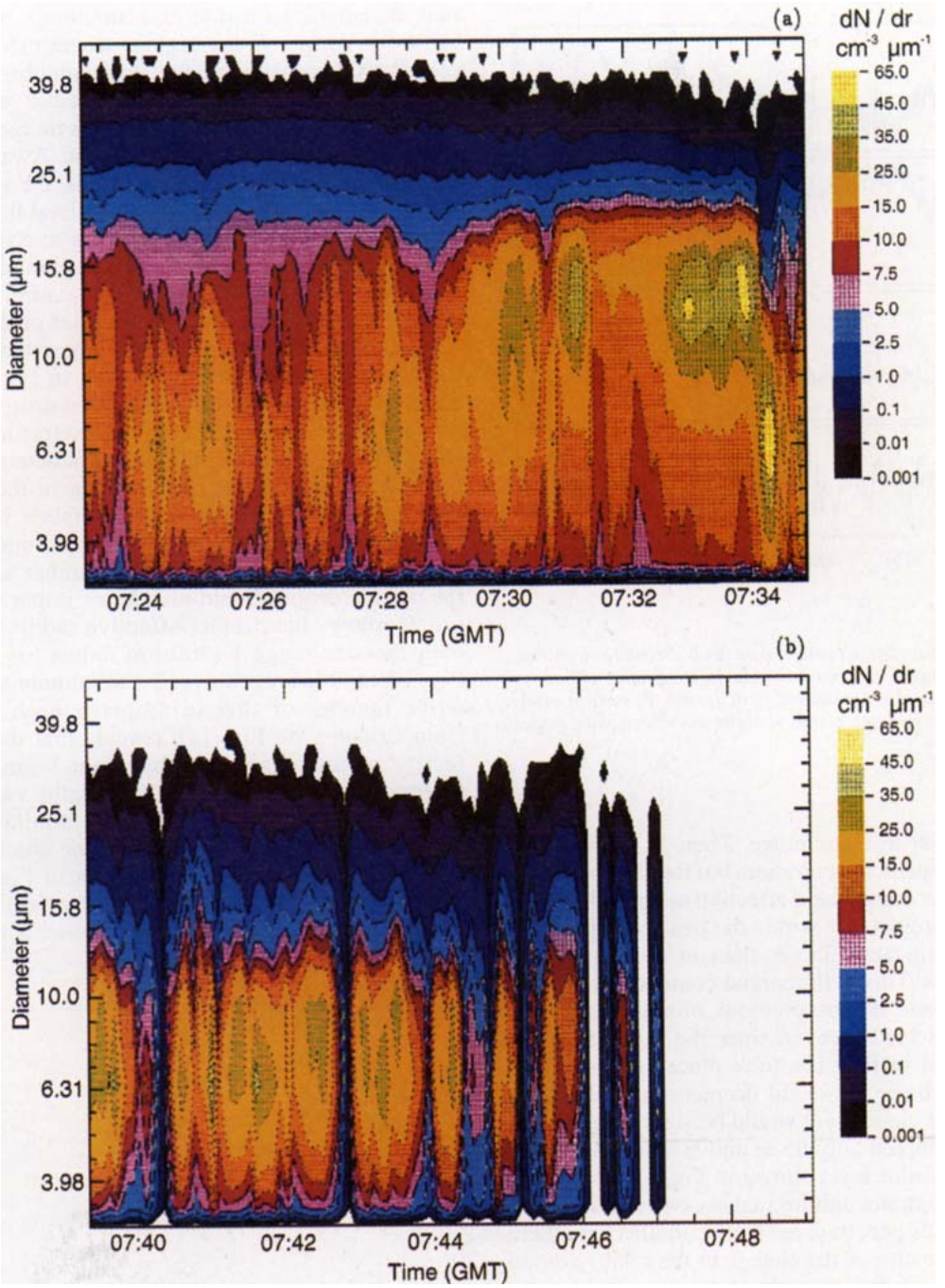

FIG. 10. Contoured droplet size distributions from a Particle Measuring Systems (PMS) Forward Scattering Spectrometer Probe (FSSP) for the size range 3.2–48.7-μm diameter, measured during horizontal runs in stratocumulus at (a) 0730 UTC 19 June 1992 at a height of 1700 m and (b) 0745 UTC 20 June 1992 at a height of 2010 m. The spectra have been averaged over 5-s intervals, and the contour values are dN/dr in cm^{-3} μm^{-1}.

encountered in these two runs (Figs. 10a and 13a) were sampled at similar heights above cloud base.

Comparison of Fig. 13a with Fig. 10a reveals that although the peaks in the droplet size distributions within the cumulus clouds both occur at approximately the same droplet diameter, the difference between the cumulus and stratocumulus droplet spectra in Fig. 13a is far more marked than that in Fig. 10a. Figures 13b–d show the corresponding time series of droplet concentration, liquid water content, and effective radius

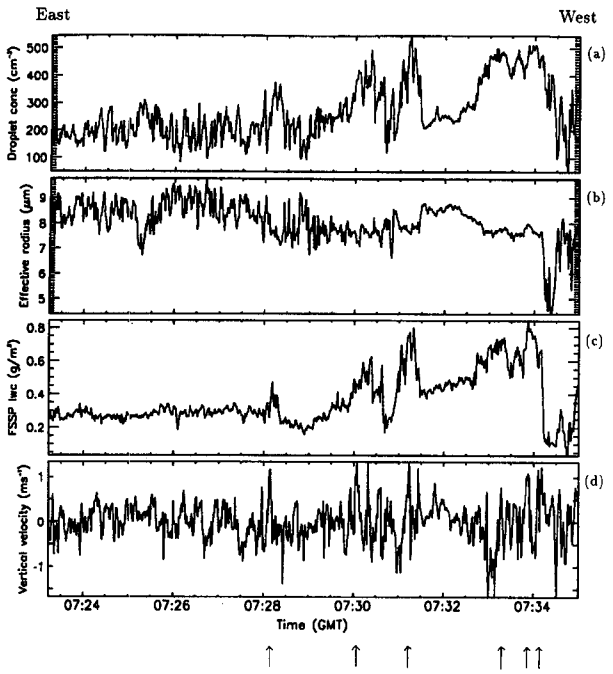

FIG. 11. Measurements made during the horizontal run shown in Fig. 10a: (a) droplet concentration (cm^{-3}), (b) droplet effective radius (μm), (c) liquid water content (g m^{-3}), and (d) vertical velocity (m s^{-1}). Arrows indicate active updrafts associated with cumulus cloud penetration.

calculated over this size range. There is no significant change in droplet concentration, but the sharp increases in liquid water content and effective radius confirm that the average droplet size within the penetrating cumulus cloud is significantly larger than in the surrounding stratocumulus. This is in marked contrast with the observations made on the previous morning, shown in Figs. 10a and 11. However, since the run in the cloud layer sampled in Fig. 10a took place at least 150 m above cloud base, the cloud droplets sampled in that stratocumulus cloud layer would be significantly larger than those sampled only 65 m above cloud base in the thin stratocumulus layer shown in Fig. 13. The microphysics of the stratocumulus in these two regions where cumulus clouds penetrate the stratocumulus base therefore differ because of the change in the relative cloud-base heights of the two cloud types and are most marked when this difference is greatest.

The lateral variation in thickness of the cloud layer in Fig. 10a is illustrated in Fig. 14, which shows a time series of the cloud liquid water path, measured with a microwave radiometer (English et al. 1994; Taylor and English 1995) during a run below the cloud layer at 0630 UTC on 19 June. The liquid water path more than doubles along the run, as the region where cumulus clouds are penetrating the stratocumulus is approached. Observations made during horizontal runs on the morning of 19 June, both upwind and across wind, indicated that the cumuli tended to exist in clumps of the order of 30 km across. In the regions where many cumulus clouds were penetrating the stratocumulus, the cloud layer was thicker and the liquid water path consequently higher as the cumulus clouds merged with and spread out into the stratocumulus base. Away from this region of penetrating cumulus clouds, the stratocumulus cloud base was higher, and the cloud thinner.

These observations show that the microphysics of a stratocumulus layer into which cumulus clouds grow may vary considerably, both spatially and temporally. Figure 15 shows a time series of the concentration (number/liter) of drops larger than 175-μm diameter, measured during the run in Fig. 10a. The concentrations of these drizzle-sized drops are small and are lower within the area of penetrating cumulus clouds than in the surrounding stratocumulus, with the lowest concentrations occurring in the most active updrafts. Since the larger droplets in the size spectrum will strongly influence the cloud's optical properties, the variations in the number and size of the drizzle drops should also be of importance. Figure 16 shows the droplet effective radius calculated over the size range 1–400 μm radius for the run in Fig. 10a and averaged over 5 s to include a representative number of drizzle drops in each spectrum. Comparison with Fig. 11b reveals that the total effective radius is increased by about 1 μm when the larger drops are included. However, the variations in effective radius along the run are similar to those seen in Fig. 11b. This shows that the changes in the concentration of drizzle drops seen in Fig. 15 have less influence on the total droplet effective radius than the variations in the relative concentrations of

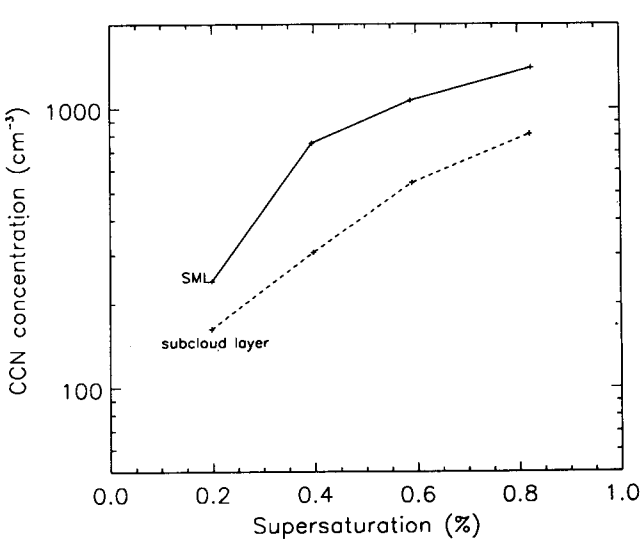

FIG. 12. CCN activity spectra measured using a thermal gradient diffusion chamber (Saxena and Kassener 1970) in the SML at 0825 UTC on 19 June at a height of 30 m (solid line) and in the subcloud layer at 0912 UTC 19 June at a height of 1380 m (dashed line).

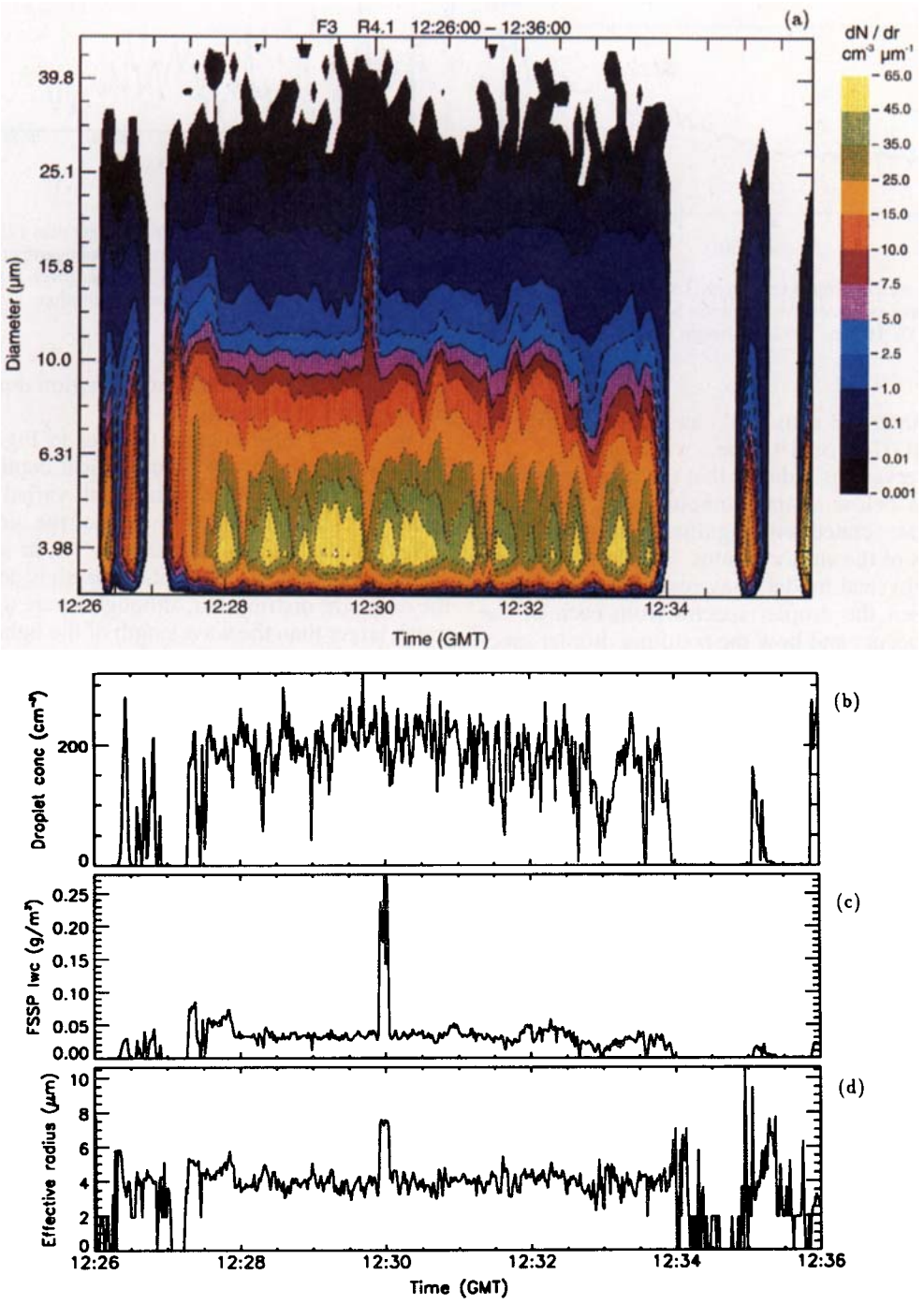

FIG. 13. Measurements made using a PMS FSSP during a horizontal run in a thin layer of stratocumulus at 1230 UTC on 20 June 1992 at a height of 1815 m. (a) Contoured droplet size distributions for the size range 3.2–48.7-μm diameter. The spectra have been averaged over 5-s intervals, and the contour values are dN/dr in cm^{-3} μm^{-1}. (b) Droplet concentration (cm^{-3}). (c) Liquid water content (g m^{-3}). (d) Droplet effective radius (μm) calculated over the size range 3.2–48.7-μm diameter.

droplets in the size range 1–48-μm seen in Figs. 10a and 13a. This is because the concentration of drizzle drops is very low ($\sim$0.001 cm^{-3}) compared with that of the cloud droplets ($\sim$100 cm^{-3}), and the drizzle rates [calculated using fall velocities given by Beard (1976)] from these clouds are therefore extremely

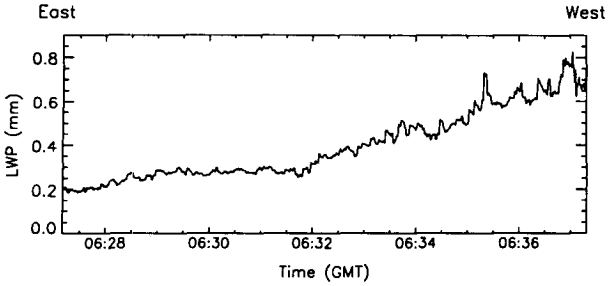

FIG. 14. Time series of liquid water path (LWP) measured remotely using a microwave radiometer during a run below the stratocumulus layer at 0630 UTC 19 June 1992 at a height of 1050 m.

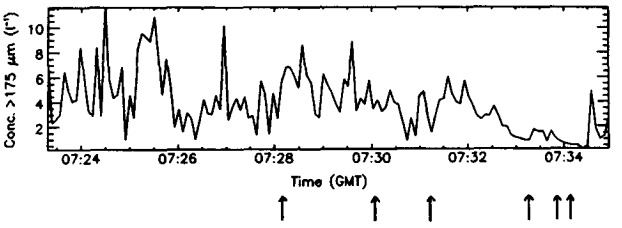

FIG. 15. Concentration (L^{-1}) of drops larger than 175-μm diameter measured with a PMS 2D cloud probe (Baumgardner 1989) during the run in Fig. 10a. The data are averaged over 5 s. The arrows indicate the regions of cumulus cloud penetration.

small (less than 0.3 mm h^{-1}), as shown in Fig. 17 for the run at 0730 on 19 June.

These observations indicate that the presence of cumulus clouds below a stratocumulus layer and rising up into it is associated with significant changes in the microphysics of the stratocumulus. Further studies, using a microphysical model, may reveal how the interaction between the droplet spectra from each of the cloud types occurs and how the resulting droplet spectrum develops. These will be reported on in a future paper.

4. Satellite analyses

Changes in cloud microphysics will ultimately affect the radiative properties of the cloud layer and hence the surface energy budget. Therefore, if the microphysics of a stratocumulus cloud layer is different in regions where cumulus clouds interact with the stratocumulus from that in surrounding regions, and if this situation is widespread, it could influence the radiation budget of the earth as a whole. Satellite images can be used to examine the influence of the presence of cumulus clouds on the radiative properties of the stratocumulus. The cloud optical depths in Figs. 18a–e and the low cloud (defined as cloud tops below 4 km) amounts in Figs. 19a–f were derived from 5-km resolution Meteosat visible (0.5–0.9 μm) and infrared (10.5–12.5 μm) images using the methods described by Minnis et al. (1992) and Minnis et al. (1987), respectively. The values were averaged on a grid from 38.5° to 31.0°N and from 24.0° to 20.0°W at a resolution of 0.5 degrees. The grid values have been contoured to give an overall view, and regions where the cloud-top height was greater than 2500 m (i.e., where cloud was present above the boundary layer) have been set to zero. The sharp gradients in optical depth and cloud amount at the edges of the graphs and around the regions of high cloud are an artifact of the contouring routine. The location of the air parcel at each time during the Lagrangian experiment has been marked on each graph (box), and the variations in the cloud conditions within this air parcel and in the surrounding region during the period can be seen clearly.

One of the most notable features in Fig. 18a is the lateral variability of the cloud optical depth in this region. At this time, the optical depth varied from more than 16.0 within the western part of the air parcel followed by the aircraft to less than 3.0 in some of the surrounding regions. The optical depth is dependent on the drop size distribution, although where the drops are much larger than the wavelength of the light the optical depth is proportional to liquid water path (LWP) and inversely proportional to droplet effective radius (r_e):

$$\tau \approx \frac{3}{2}\frac{\mathrm{LWP}}{\rho_w r_e} \tag{2}$$

(Stephens 1978), where ρ_w is the density of water,

$$\mathrm{LWP} = \int_{z_b}^{z_t} q_l(z)\,dz, \tag{3}$$

where $q_l(z)$ is the cloud liquid water content at height z and r_e is given by Eq. (1). An increase in optical depth therefore implies either an increase in LWP or a decrease in r_e or both. The aircraft measurements described in section 3b showed that cumulus clouds penetrated and spread out into the stratocumulus in the western part of the air parcel on the morning of 19 June, and the cloud thickness (and hence the liquid water path) in this region was considerably greater while the droplet effective radius was smaller than in the surrounding regions. Thus, it is likely that the area of

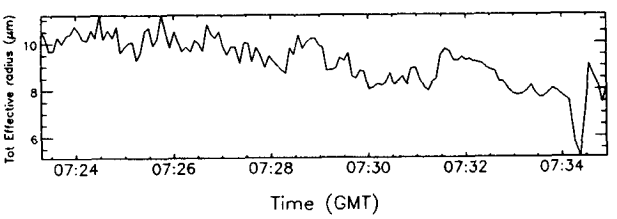

FIG. 16. Droplet effective radius calculated over the size range 1–400-μm radius using combined spectra from the FSSP and 2D cloud probe, which were averaged over 5 s for the run in Fig. 10a.

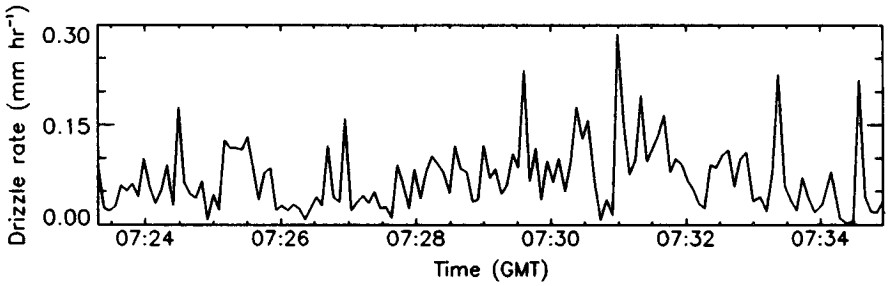

FIG. 17. Drizzle rate for droplets larger than 175-μm diameter (measured with a PMS 2D cloud probe) calculated using fall velocities given by Beard (1976) for the horizontal run in the stratocumulus at 0730 UTC 19 June 1992 (Fig. 15).

greater optical depth in the air parcel shown in Fig. 18a is associated with the presence of this clump of cumulus clouds below the stratocumulus. This implies that although the penetration of the stratocumulus by an individual cumulus cloud would not be resolved by a satellite measurement, the occurrence of the cumulus clouds in clumps tens of kilometers across, and the effects of lateral mixing of the cumulus cloud effects within the stratocumulus, could be associated with variations in the radiative properties of the stratocumulus on a much larger scale and could be observed by a satellite.

Figures 18a–e show that within the air parcel followed by the aircraft during the period of this Lagrangian experiment (box) the cloud optical depth decreased significantly after the morning of the 19 June. Although the higher optical depths associated with the presence of the cumulus cloud clump observed early on 19 June are still apparent at 1400 UTC (Fig. 18b), they are far less marked than in Fig. 18a and almost disappear by 1800 UTC (Fig. 18c). This is shown more clearly in Fig. 18f. Here, the values of optical depth in each of the four gridboxes between 21° and 23°W covering the location of the air mass at each available time (approximately every half hour from 0800 to 1800 UTC on 19 June and from 0800 to 1400 UTC on 20 June) have been averaged and plotted against time. (Where any gridbox was known to contain cloud above 2500 m, the optical depth for that gridbox was not included in the average.) It can be seen that the average optical depth decreases from about 18 to 3 during the period. This is coincident with the observed decrease in the number of cumulus clouds penetrating the stratocumulus during the period and with the change in the characteristics of the free tropospheric air above the stratocumulus (section 3a).

It was noted in section 3b that the stratocumulus was thicker in the regions where cumuli were interacting with the cloud layer than in the intervening regions. The distribution of low cloud amount in Fig. 19a indicates that there is a slight increase in cloud fraction in the region of cumulus cloud penetration within the air parcel followed by the aircraft compared with the surrounding regions, but, that this change is less marked than the differences in cloud microphysics and vertical extent that contribute to the increased optical depth in Fig. 18a. There is no clear increase or decrease in low cloud amount within the air parcel over time in Figs. 19a–f, and the averages shown in Fig. 19g indicate that the average cloud amount in the air parcel varies almost randomly during the period. This implies that for a stratocumulus layer where clumps of cumulus clouds are interacting with certain regions of the cloud while other regions remain unaffected, it is mainly the cloud microphysics and vertical extent, and hence the radiative properties, that show corresponding variations rather than the cloud fraction. The observation that this occurs on a scale large enough to be measured by satellite at 0.5 degrees resolution suggests that this interaction may have an important influence on the radiation budget.

5. Discussion

Observations made during a 34-h Lagrangian study highlight some of the features of a marine boundary layer in which cumulus clouds are generated below stratocumulus and subsequently penetrate the cloud layer. These can be summarized as follows:

(a) The cumulus clouds are associated with upward transport of air from the SML into the stratocumulus cloud layer. The values of θ_e and q_T in the SML are usually higher than those in the subcloud and cloud layers, so localized increases in these variables are observed when the cumulus clouds penetrate the cloud layer.

(b) The stratocumulus layer is thicker in regions where cumulus clouds penetrate. We suggest that this is due to the cumulus clouds merging with and spreading out into the cloud layer.

(c) In this polluted air mass, the intrusion of cumulus clouds results in localized increases in droplet concentration and liquid water content in the stratocumulus cloud layer. Consequently, there is a local decrease in the maximum cloud droplet size, as more droplets compete for the available water vapor.

(d) The variations in the stratocumulus microphysics that are associated with penetrating cumulus clouds

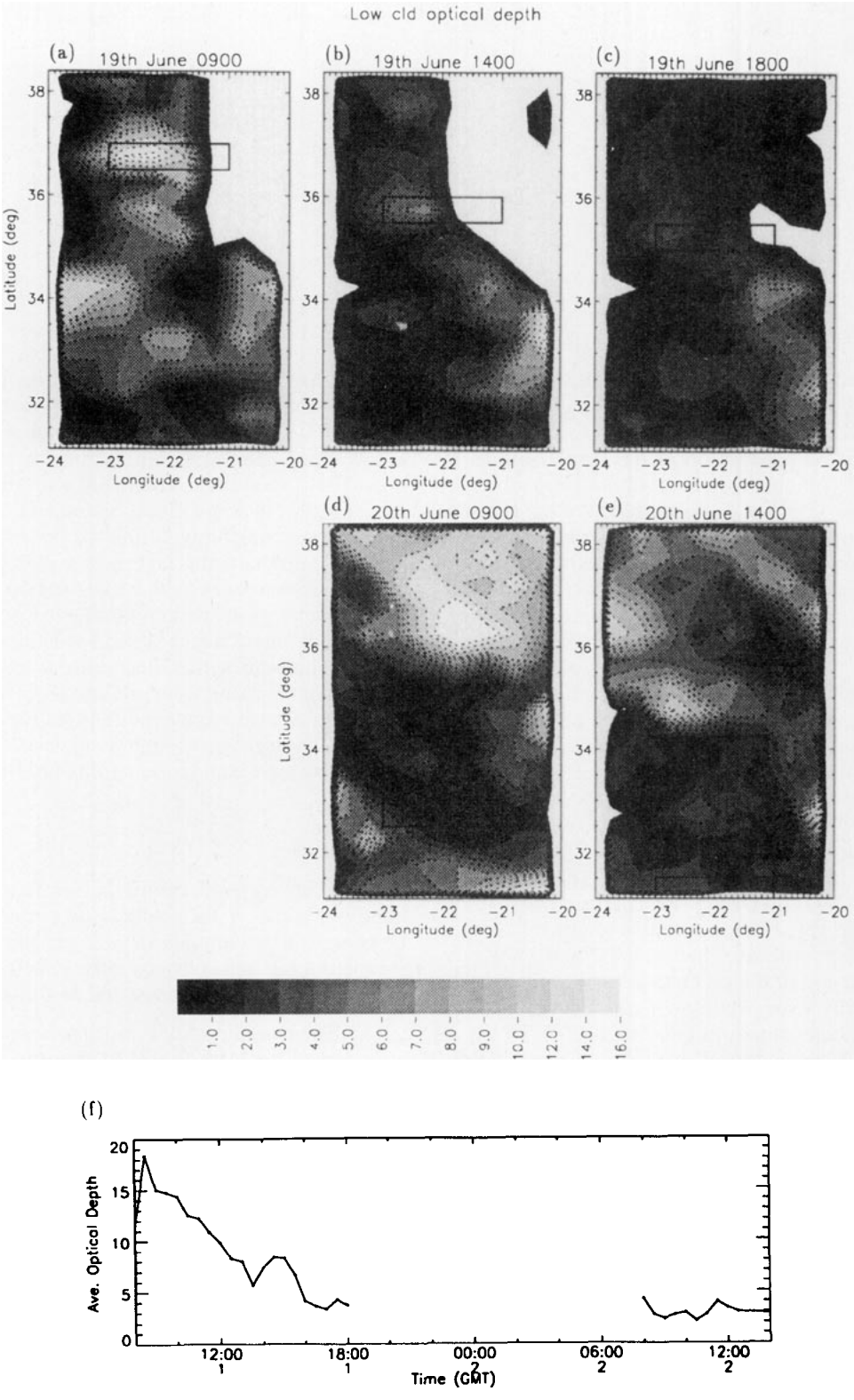

FIG. 18. (a–e) Low cloud optical depths derived from Meteosat visible images averaged on a grid from 38.5° to 31.0°N and from 24.0° to 20.0°W at a resolution of 0.5 degrees. See text for full description. The box indicates the location of the air parcel followed by the aircraft during this experiment. (f) Low cloud optical depth averaged over the four gridboxes between 21° and 23°W covering the location of the air mass at each available time between 0800 UTC 19 June 1992 and 1400 UTC 20 June.

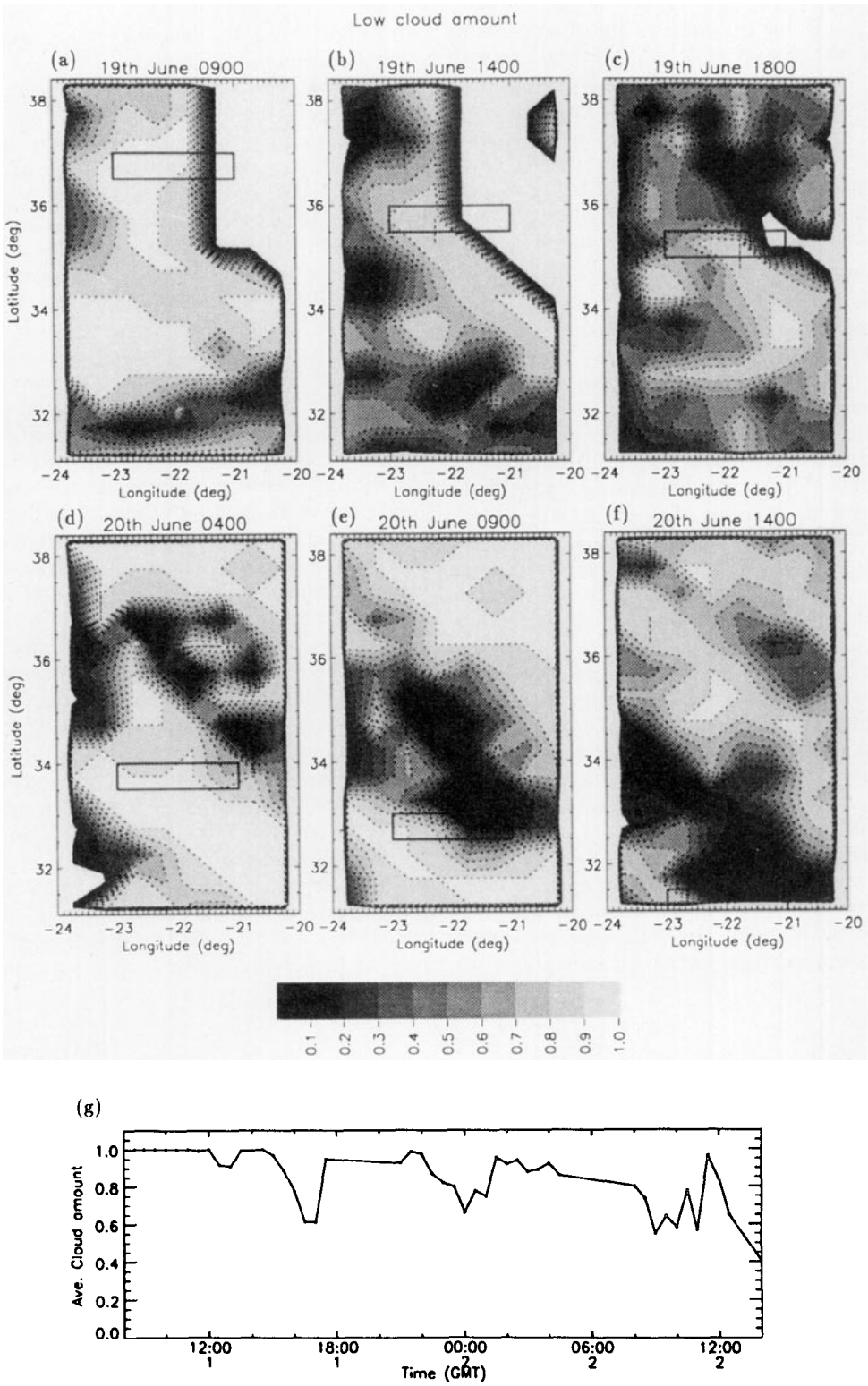

FIG. 19. (a–f) Low cloud amounts derived from Meteosat infrared images averaged on a grid from 38.5° to 31.0°N and from 24.0° to 20.0°W at a resolution of 0.5 degrees. See text for full description. (g) Low cloud amount averaged over the four gridboxes between 21° and 23°W covering the location of the air mass at each available time between 0800 UTC 19 June 1992 and 1400 UTC 20 June.

differ according to the thickness of the stratocumulus layer relative to the maximum depth of the cumulus clouds.

(e) The optical depth of the stratocumulus cloud is greater in the vicinity of the cumulus cloud penetration and is likely to be associated with the greater cloud liquid water path and smaller droplet effective radius.

(f) Drizzle amounts are lower in regions of active cumulus penetration in this polluted air mass.

Figure 20 summarizes these observations. Several observations of this type of cloud structure were also made on Santa Maria during ASTEX using a 94-GHz cloud radar (Miller and Albrecht 1995), which indicates good agreement between the aircraft- and surface-based measurements.

It should be emphasized that these observations of cumulus–stratocumulus interaction are from a single case study, and, while similar observations were made on several other days during ASTEX, it is not clear whether this behavior would be repeated in another stratocumulus layer in, for example, a different location or a different air mass. Additionally, given the nature of this dataset, we cannot say definitively what processes are occurring in this boundary layer in which cumulus clouds are interacting with the stratocumulus. However, we feel it is reasonable to suggest that the cumulus clouds influence both the thermodynamic and microphysical properties of the stratocumulus layer. We suggest that the cumulus clouds may have been helping to maintain and reinforce the stratocumulus locally in a boundary layer in which vertical mixing from the sea surface to the cloud layer was inhibited. The thinner cloud layer observed on the morning of 20 June, when visual observations indicated that no cumulus penetrated the cloud layer, could then be associated both with the changes in the thermodynamic properties of the air above the boundary layer and the lack of penetrating cumulus clouds.

It is also possible to make some suggestions as to which aspects of the boundary-layer conditions may influence what is observed in a particular region in which cumulus clouds are interacting with a stratocumulus cloud layer. The airmass type may determine whether the droplet size and concentration are increased or decreased locally, when the cumulus clouds penetrate. This may affect the radiative properties of the cloud layer, although the increase in liquid water content and cloud thickness also associated with the penetrating cumulus clouds may increase the cloud reflectivity even if the droplet size increases. The shape of the CCN activity spectrum associated with a particular air mass may determine the extent to which the cloud droplet concentration is affected by changes in the updraft velocity. Where the CCN spectra have lower slopes than those observed in this case study, such as may be observed in a cleaner air mass, the cloud droplet number concentration will be less sensitive to variations in the updraft. The introduction, by the cumulus clouds, of droplets that are of a different size than those already existing in the stratocumulus may provide the differential fall velocities necessary for coalescence, thus providing the potential for the growth of large drops. It is unlikely that significant concentrations of droplets larger than about 100 μm in diameter could grow within the lifetime of a penetrating cumulus cloud. It is possible, however, that the interaction between the cumulus and stratocumulus clouds could initiate the formation of droplets larger than about 40-μm diameter by coalescence, which may subsequently grow to drizzle size after the cumulus clouds have decayed. This could be aided by an increased cloud thickness (which will provide a greater depth of cloud

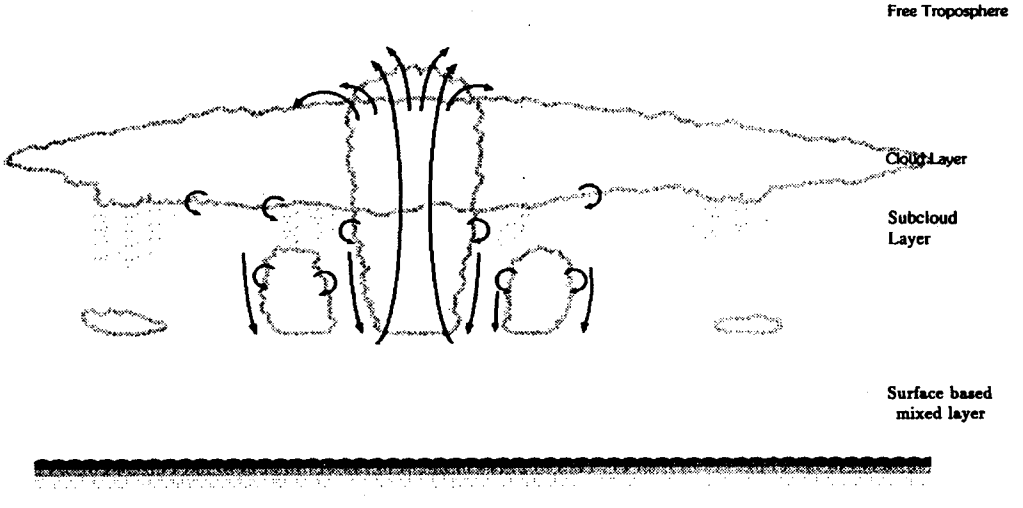

FIG. 20. Schematic representation of the processes thought to be occurring when cumulus clouds interact with a decoupled stratocumulus layer over the sea.

through which the larger drops can fall) and by increased turbulent motions associated with subsequent penetrating cumulus clouds [which could simply enable some of the larger drops to remain in the cloud for a sufficient length of time that drizzle drops can grow by stochastic coalescence (Mason 1952; Nicholls 1987)]. The extent to which the cumulus–stratocumulus interaction could be associated with enhanced drizzle formation may depend on the airmass type, since this will influence the size of cloud droplets in both the cumuli and the stratocumulus and hence the timescale for the growth of large drops. If drizzle formation is enhanced, this could affect the water content of the cloud and hence its radiative properties. Continued precipitation will deplete the cloud liquid water content, which will not only decrease the cloud reflectivity (Slingo 1989), but could allow the cloud layer to break up. It is therefore important to fully investigate the possible impact of the cumulus–stratocumulus interaction on drizzle in the stratocumulus over all timescales.

It is possible that the effects of cumulus–stratocumulus interaction may persist for some time after the cumulus clouds have decayed away, although lateral and vertical mixing may dilute the sharp changes in droplet size and concentration, so that new penetrations by cumulus clouds would still appear as sharp spikes in the microphysical parameters. We suggest that the higher background values of θ_e and q_T in the stratocumulus in Fig. 8 may be a result of previous penetrations of the stratocumulus layer by cumulus clouds. If no further penetrations by cumulus clouds occur for some time, and the stratocumulus persists, it is possible that the microphysics in the stratocumulus layer could eventually return to the more classic description, where the droplet concentration is approximately uniform in the cloud layer, but the liquid water content and the average droplet size increase with height almost adiabatically. There may therefore be considerable differences in cloud microphysics between regions of a cloud layer that have been affected by cumulus cloud penetration at different times during their evolution. Alternatively, if the cumulus clouds penetrating another stratocumulus layer are more vigorous than those observed in this study, entrainment of free tropospheric air into the cloud layer could be sufficiently enhanced in the vicinity of the cumulus clouds, particularly if they overshoot the stratocumulus top and distort the temperature inversion, so that a rapid break up of the stratocumulus layer results (Nicholls 1984; Bretherton 1992).

The cumulus–stratocumulus interaction is therefore complex, and several questions remain to be answered. It is important to fully understand the relationship between the presence of penetrating cumulus clouds and the structure of the boundary layer, since the interaction may be inherent in the transition from stratocumulus to trade wind cumulus. The microphysical interaction requires further investigation, with the aid of a microphysical model, to understand how the droplet size distribution in the stratocumulus changes and under what conditions and on what timescale the growth of larger drops could occur. The sensitivity of the microphysical interaction to the aerosol concentration in the boundary layer must be ascertained. Similarly, the effects of the clouds on the size and concentration of the aerosol particles should be fully investigated. Since all of these aspects of the cumulus–stratocumulus interaction have some effect on the radiative transfer properties of the stratocumulus, it may be necessary to produce parameterizations of these effects for use in large-scale numerical models.

Acknowledgments. We would like to thank the scientists and aircrews of the Meteorological Research Flight, the NCAR Electra, and the University of Washington C-131. The National Center for Atmospheric Research is supported by the National Science Foundation. We also thank S. English for processing the microwave spectrometer data from the C-130 and providing the LWP measurements, David R. Doelling and Rabindra Palikonda for their assistance in analyzing the satellite data, and P. Austin for supplying drizzle measurements from the NCAR Electra. Partial funding for the satellite analyses was provided by the Office of Naval Research under Grant USN-N0001491IMP24011. G. M. Martin was supported by a consortium of oil companies within the International Petroleum Industry Environment Conservation Association (IPIECA). D. P. Rogers was supported by the Office of Naval Research Marine Meteorology Program N00014-90-J-1265.

REFERENCES

Albrecht, B. A., 1989: Aerosols, cloud microphysics and fractional cloudiness. *Science,* **245,** 1227–1230.

——, R. S. Penc, and W. H. Schubert, 1985: An observational study of cloud-topped mixed layers. *J. Atmos. Sci.,* **42,** 800–822.

——, D. A. Randall, and S. Nicholls, 1988: Observations of marine stratocumulus during FIRE. *Bull. Amer. Meteor. Soc.,* **69,** 618–626.

——, C. S. Bretherton, D. W. Johnson, W. H. Schubert, and A. S. Frisch, 1994: The Atlantic Stratocumulus Transition Experiment—ASTEX. *Bull. Amer. Meteor. Soc.,* **76,** 889–904.

Baumgardner, D., 1989: Airborne measurements for cloud microphysics. NCAR Research Aviation Facility Bulletin 24. [Available from NCAR, P.O. Box 300, Boulder, CO 80307.]

Beard, K. V., 1976: Terminal velocity and shape of cloud and precipitation drops aloft. *J. Atmos. Sci.,* **33,** 851–864.

Bluth, R. T., and B. A. Albrecht, 1993: ASTEX and MAGE Experiment summary. Part I—Mission Summaries. The Pennsylvania State University, Dept. of Meteorology, University Park, PA, 286 pp.

Blyth, A. M., 1993: Entrainment in cumulus clouds. *J. Appl. Meteor.,* **32,** 626–641.

Bougeault, P., 1985: The diurnal cycle of the marine stratocumulus layer. A higher-order model study. *J. Atmos. Sci.,* **42,** 2826–2843.

Bower, K. N., and T. W. Choularton, 1992: A parametrisation of the effective radius of ice free clouds for use in global climate models. *Atmos. Res.,* **27,** 305–339.

Bretherton, C. S., 1992: A conceptual model of the stratocumulus-trade-cumulus transition in the subtropical oceans. *Proc. 11th Int. Conf. on Clouds and Precipitation,* Vol. 1, Montreal, Quebec, Canada, International Commission on Clouds and Precipitation and International Association of Meteorology and Atmospheric Physics, 374–377.

English, S. J., C. Guillou, C. Prigent, and D. C. Jones, 1994: Aircraft measurements of water vapour continuum absorption at millimetre wavelengths. *Quart. J. Roy. Meteor. Soc.,* **120,** 603–625.

Foot, J. S., 1988: Some observations of the optical properties of clouds. I: Stratocumulus. *Quart. J. Roy. Meteor. Soc.,* **114,** 129–144.

Hanson, H. P., 1991: Cloud albedo control by cloud-top entrainment. *Tellus,* **43A,** 37–48.

Hobbs, P. V., L. F. Radke, J. H. Lyons, R. J. Ferek, D. J. Coffman, and T. J. Casadevall, 1991: Airborne measurements of particle and gas emissions from the 1990 volcanic eruptions of Mount Redoubt. *J. Geophys. Res.,* **96,** 18 735–18 752.

James, D. G., 1959: Observations from aircraft of temperatures and humidities near stratocumulus clouds. *Quart. J. Roy. Meteor. Soc.,* **85,** 120–130.

Johnson, D. W., G. M. Martin, J. P. Taylor, C. A. Friehe, and D. P. Rogers, 1993: The effect of an outbreak of continental air from Europe on marine stratocumulus clouds near the Azores. *Proc. Spring Meeting of the American Geophysical Union,* Baltimore, MD, Amer. Geophys. Union, p. 86.

——, ——, D. P. Rogers, and C. A. Friehe, 1994: Observations of the transition from stratocumulus to trade wind cumulus during ASTEX. *Proc. Eighth Conf. on Atmospheric Radiation,* Nashville, TN, Amer. Meteor. Soc., 138–140.

Martin, G. M., D. W. Johnson, and A. Spice, 1994: The measurement and parametrisation of effective radius in warm stratocumulus clouds. *J. Atmos. Sci.,* **51,** 1823–1842.

Mason, B. J., 1952: Production of rain and drizzle by coalescence in stratiform cloud. *Quart. J. Roy. Meteor. Soc.,* **78,** 377–386.

Miller, E. R., and R. B. Friesen, 1989: Standard output data products from the NCAR Research Aviation Facility. NCAR Research Aviation Facility Bull. 9, 70 pp. [Available from NCAR, P.O. Box 3000, Boulder, CO 80307.]

Miller, M. A., and B. A. Albrecht, 1995: Surface-based remote sensing of mesoscale cloud structure during ASTEX. *J. Atmos. Sci.,* **52,** 2809–2826.

Minnis, P., E. F. Harrison, and G. G. Gibson, 1987: Cloud cover over the eastern equatorial Pacific derived from July 1983 ISCCP data using a hybrid bispectral threshold method. *J. Geophys. Res.,* **92,** 4051–4073.

——, P. W. Heck, D. F. Young, C. W. Fairall, and J. B. Snider, 1992: Stratocumulus cloud properties derived from simultaneous satellite and island-based instrumentation during FIRE. *J. Appl. Meteor.,* **31,** 317–339.

Nicholls, S., 1984: The dynamics of stratocumulus: Aircraft observations and comparisons with a mixed layer model. *Quart. J. Roy. Meteor. Soc.,* **110,** 783–820.

——, 1987: A model of drizzle growth in warm, turbulent, stratiform clouds. *Quart. J. Roy. Meteor. Soc.,* **113,** 1141–1170.

——, and J. R. Leighton, 1986: An observational study of the structure of stratiform cloud sheets: Part I. Structure. *Quart. J. Roy. Meteor. Soc.,* **112,** 431–460.

——, B. Brummer, F. Fieldler, A. Grant, T. Hauf, G. Jenkins, C. Readings, and W. Shaw, 1983: The structure of the turbulent atmospheric boundary layer (during JASIN). *Philos. Trans. Roy. Soc. London, Ser. A,* **308,** 291–309.

Noonkester, V. R., 1984: Droplet spectra observed in marine stratocumulus cloud layers. *J. Atmos. Sci.,* **41,** 829–845.

Paluch, I. R., 1979: The entrainment mechanism in Colorado cumuli. *J. Atmos. Sci.,* **36,** 2467–2478.

——, and D. H. Lenschow, 1991: Stratiform cloud formation in the marine boundary layer. *J. Atmos. Sci.,* **48,** 2141–2158.

Rogers, D. P., and J. W. Telford, 1986: Metastable stratus tops. *Quart. J. Roy. Meteor. Soc.,* **112,** 481–500.

——, and D. Koračin, 1992: Radiative transfer and turbulence in the cloud-topped marine atmospheric boundary layer. *J. Atmos. Sci.,* **49,** 1473–1486.

——, D. W. Johnson, and C. A. Friehe, 1995a: The stable internal boundary layer over a coastal sea. Part I. Airborne measurements of the mean and turbulence structure. *J. Atmos. Sci.,* **52,** 667–683.

——, X. Yang, P. M. Norris, D. W. Johnson, G. M. Martin, C. A. Friehe, and B. W. Berger, 1995b: Diurnal evolution of the cloud-topped marine boundary layer. Part I. Nocturnal stratocumulus development. *J. Atmos. Sci.,* **52,** 2953–2966.

Rogers, R. R., and M. K. Yau, 1989: *A Short Course in Cloud Physics.* 3d ed. Pergamon Press, 293 pp.

Saxena, V. K., and J. L. Kassener Jr., 1970: Thermal gradient diffusion chambers as cloud-nuclei counters. *Proc. Symp. on Precipitation Scavenging,* Washington, D.C., U.S. Atomic Energy Commission 217–238.

Slingo, A., 1989: A GCM parameterization for the shortwave radiative properties of water clouds. *J. Atmos. Sci.,* **46,** 1419–1427.

——, S. Nicholls, and J. Schmetz, 1982: Aircraft observations of marine stratocumulus during JASIN *Quart. J. Roy. Meteor. Soc.,* **108,** 833–856.

Stephens, G. L., 1978: Radiation profiles in extended water clouds. II: Parameterization schemes. *J. Atmos. Sci.,* **35,** 2123–2132.

Taylor, J. P., and S. J. English, 1995: The retrieval of cloud radiative and microphysical properties using combined near infra-red and microwave radiometry. *Quart. J. Roy. Meteor. Soc.,* in press.

Turton, J. D., and S. Nicholls, 1987: A study of the diurnal variation of stratocumulus using a multiple mixed layer model. *Quart. J. Roy. Meteor. Soc.,* **113,** 969–1009.